Supplemental Material to the Manuscript "Permanent reduction of dissipation in nanomechanical Si resonators by chemical surface protection"

Y. Tao[1,2], P. Navaretti[1,3], R. Hauert[4], U. Grob[1], M. Poggio[3], and C. L. Degen[1]

[1]Department of Physics, ETH Zurich, Schafmattstrasse 16, 8093 Zurich, Switzerland.

[2]Department of Chemistry, Massachusetts Institute of Technology, 77 Massachusetts Avenue, Cambridge MA 02139, USA.

[3]Department of Physics, University of Basel, Klingelbergstrasse 82, 4056 Basel, Switzerland.

[4]Empa, Swiss Federal Laboratories of Materials Science and Technology, Ueberlandstrasse 129, 8600 Duebendorf Switzerland.

Contents

1. Guide to the Document **2**

2. Review of Surface Reactions on Single-Crystal Silicon **3**

3. Experimental Methods **5**

4. Tabulation of Key Results **9**

5. Quality Factor vs Temperature for Some Important Samples **10**

6. X-ray photoelectron spectroscopy (XPS) Analysis of Silicon Surfaces **12**

7. Frequency and Quality Factor Data from Cyclic Oxide Removal-Native Oxidation Experiments **17**

8. Si and SiO_2 Material Properties Used in Data Analysis **18**

9. Oxide Growth Underneath Polydimethylsiloxane Thin Film **19**

10. Other Tested Silicon Surface Modification Strategies With Results That May be Optimized **21**

10.1. Two-Step Alkylation and Amination Reactions (IIa) 21

10.2. Spontaneous Diazonium Salt Grafting (IIa) 21

10.3. Atomic Layer Deposition (ALD) of Al_2O_3 (IIc) 21

10.4. Electron Beam Evaporation of Al_2O_3 (IIc) 22

10.5. Simultaneous Exposure to HF Vapor and Alkene Vapor 22

1. Guide to the Document

This section briefly introduces the content of this document to facilitate the retrieval of information.

(i) The work presented in the main manuscript are hits from a quasi-exhaustive screening of existing silicon surface modification technology. A short review-style classification of this technology is provided in Section 2. to help the reader gain an overview of the field.

(ii) Section 3. provides the full experimental procedure.

(iii) Section 4. and accompanying Table 1 summarizes the key measurement results on promising surface protection strategies identified in the current study.

(iv) Section 5. gives examples of Q or Q^{-1} vs T plots for important surface terminations investigated. A selection of these are presented in Figure 6 of the main manuscript.

(v) Section 6. provide summary of x-ray photoelectron spectroscopy (XPS) characterization results on all novel surfaces prepared and reported in this study.

(vi) Sections 7. and 8. provides additional details about the methods used to study the mechanical properties of the native oxide layer, as discussed in the main text in Figure 2c and 2d.

(vii) Section 9. provides the data, model, and calculation method used to show that native oxide continues to grow in air after the treatment with dichlorodimehtylsilane. This is relevant to Figure 5 of the main text.

(viii) Section 10. discusses several surface treatment strategies. Some of these may be optimized further. Others provides additional information about the behavior of the system that may be of interest to future workers.

2. Review of Surface Reactions on Single-Crystal Silicon

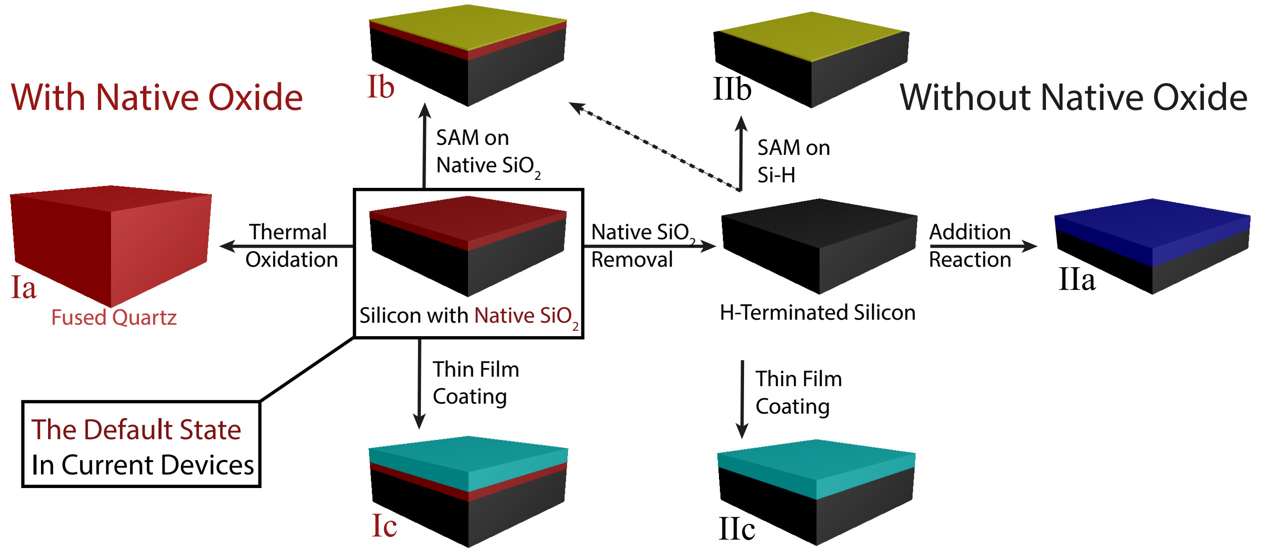

Figure A: Conceptual Overview of Strategies for Silicon Surface Modification.

The surface chemistry of single-crystal silicon has been developed extensively in the last sixty years. Methods can be divided into two major categories depending on the presence (**I**) or the absence (**II**) of the native oxide layer (Figure A). One can conceptually envision at least three sub-categories of strategies for both **I** and **II**: (**a**) growing a dielectric layer of controlled thickness by the reaction of the resident silicon crystal lattice with other elements, (**b**) forming a self-assembled monolayer (SAM), and (**c**) depositing an arbitrary thin film(s) of controlled thickness, crystalline or amorphous, by any available method.

A native oxide-covered surface is the default state for current silicon devices (Rectangle in Figure A). From this starting point, the simplest example of dielectric layer growth (**Ia**) is the thermal oxidation of silicon [1]. We investigated this process to qualitatively compare the bulk dissipative property of amorphous SiO_2 with that of LPCVD Si_3N_4 (Figure B). SAM formation (**Ib**) is generally based on S_N2 reaction between incoming electrophiles and resident Si-OH nucleophile on the surface. Chlorosilanes, alkoxylsilanes, and silazanes are the most common types of electrophiles in such a silanization strategy that alters surface properties such as surface friction and surface energy, but conserves the properties of the bulk substrate as originally found in the defect-rich Si/SiO_x bimorph. For the purpose of improving Q and electrical performance of silicon NEMS, both intuition and a relevant literature report [2] seem to argue against the utility of this approach. Unexpectedly, however, results presented in this study show that reality may in fact be more complicated (Dashed Arrow in Figure A and Figure 5 in main text). While possibilities within **Ic** are infinite, we have refrained from pursuing this route because mechanical dissipation is additive in layered structures [3].

The second category of approaches to silicon surface modification has focused on the construction of thin dielectric layers (**IIa** and **IIc**) and of SAM (**IIb**) directly on the outermost layer(s) of lattice silicon atoms. The development of these approaches are driven on the one hand by an effort to eliminate the native oxide layer, the formation of which correlate with the degradation of certain electronic properties of the material [4, 5], and on the other hand by a quest for high-permittivity dielectric replacements to SiO_2 as a gate dielectric for DRAM and FET fabrication [6, 7].

IIa contains few possibilities, and is represented by the thermal growth of thin nitrides and oxynitrides on hydrogen-terminated silicon using either N_2 gas or NH_3 gas as the nitridizing agent [8–11]. Sub-category **IIb** is by far the most mature technology; listed approximately in decreasing order of stability to ambient conditions, Si-C, Si-O, Si-N, and Si-X (X=F, Cl, Br) bonds have been demon-

strated. Si-C bond construction has been achieved using thermal, radical-initiated, photochemical, sonochemical, or spontaneous hydrosilylation of terminal alkenes and alkynes by a H-terminated silicon surface [12–21], via the nucleophilic substitution between an activated Si-X surface [22] with a carbon nucleophile [23], via cyclocondensation on reconstructed surfaces in UHV [24], and by grafting of both carbon-centered electrophiles and nucleophiles onto Si-H surface with or without electrochemical assistance [25–28]. Most strategies leading to Si-O and Si-N linkages have proceeded under conditions analogous to those for Si-C construction, such as by hydrosilylation of an aldehyde with a Si-H surface [29, 30] and the nucleophilic substitution of activated Si-X by an oxygen- [31] or nitrogen-centered nucleophiles [32, 33]. In the case of Si-N, pericyclic modes of reactivity having no carbon and oxygen analogues have also been reported recently [34]. Finally, high-quality surfaces belonging to sub-category **IIc** are the most difficult to achieve and are prominently exemplified by the growth of thin crystalline strontium titanate ($SrTiO_3$) layers in perfect register with a silicon $<1,0,0>$ surface in dedicated molecular-beam epitaxy systems [6]. We have refrained from this last method after consulting with experts in the field, who believe that epitaxial strontium titanate is generally defect-rich and does not significantly slow down oxygen infiltration and oxidation of the silicon crystal.

3. Experimental Methods

General Reagents were purchased from Sigma-Aldrich unless otherwise specified. All solvents used in cleaning and rinsing were of HPLC grade or better. Argon was of 99.9999% purity. Nitrogen was from an in-house supply line. Glassware, Teflonware, titanium sample holders and all surfaces that may come into contact with or in the proximity of the samples and reagent liquids were rigorously cleaned in acetone, methanol, boiling piranha solution (2:1 H_2SO_4:H_2O_2), and finally DI water. Glassware and stainless steel cannula used for the purification and transfer of alkenes, alkynes, and amines were dried by dehydration bake at 300°C for >30 minutes immediately before use.

For easy handling, mm-sized cantilever chips are secured onto custom holder machined from titanium and aluminum. The holders ensured that the fragile cantilever cannot come into contact with (crash into) walls of the reactor vessels.

Fabrication The silicon cantilevers used in this experiments were fabricated from undoped SOI wafers with a 1.5 μm device layer and 1 μm of buried oxide. Procedures similar to those reported in [35] were used. The key difference is the following: The original work uses Si epitaxy from an initially-thin 0.1 μm device layer for forming the mass loading at the tip of the cantilevers. We have, instead, used ICP etching or TMAH wet etching steps from an initially thicker device layer for forming the mass loading. Our as-fabricated devices perform essentially identically to those reported in [35] in terms of frequency, spring constant, and quality factor (cf. Table 1, Section **0**).

H-termination This transformation was performed with a two-step procedure. The samples were first UV-ozone cleaned for 10 minutes to remove organic contaminants. They were then placed inside a small, custom Teflon chamber that had been thermally equilibrated to 40°C atop a hotplate. This Teflon reactor chamber is equipped with a receptacle for the hotplate's feedback thermometer as well as gas inlet/outlet valves. After 5 minutes of thermal equilibration, HF/water vapor generated in a teflon bubbler containing 49% hydrofluoric acid using N_2 as the carrier gas was flushed through the chamber at rates between 50-200 sccm for 10 minutes. Ar gas was then used to flush the chamber for 5 minutes to remove residual HF. Following exposure to air for the desired duration, the sample was mounted into the measurement setup and kept in high vacuum during measurement.

D-Termination This transformation was performed by a similar procedure, except that DF vapor was generated by bubbling N_2 through a solution of 2.0 M potassium fluoride (KF, anhydrous, powder, >99.99%) and 1.0 M sulfuric acid-d_2 (D_2SO_4, 96-98 wt.% in D_2O, 99.5 atom % D) in deuterium oxide (D_2O, >99.9 atom % D). The mixture was prepared by adding a solution of KF (0.581 g in 1.15 ml D_2O) to a solution of D_2SO_4 (0.266 ml in 3.00 ml D_2O). The N_2 gas was first dried by passing it through a $CaSO_4$ drying column to minimize proton contamination from residual H_2O vapor.

Oxide formation in the presence of different silane vapors These treatments were performed immediately following H-termination by switching the inlet feed gas to the Teflon chamber from HF vapor to silane vapor produced by gently bubbling N_2 through 1ml of the silane contained in a small glass bubbler maintained at 40°C by water bath. N_2 was passed at a gentle rate such that all of the silane evaporated in 20-30 minutes. The procedure was considered completed upon exhaustion of the liquid silane source.

Liquid-Phase Hydrosilylation The alkenes and alkyne were each dried over excess CaH_2 for two days with vigorous stirring and then distilled from CaH_2 under reduced pressure. The distillates were deoxygenated via 4 freeze-pump-thaw cycles under the high vacuum generated with a turbo-

molecular pump and finally warmed up to room temperature under a slightly positive Ar pressure. The cantilever samples were mounted onto a titanium holder, treated via the usual UV-ozone/vapor HF sequence, and quickly moved into an aluminum foil-covered 2-ml cylindrical vial (minimize light-induced oxidation before reagent addition) and tightly sealed with clamped septum. The flask was flushed with Ar for 5 min. The freshly purified alkene or alkyne was then added to the vial via cannula under slight Ar pressure to completely cover the devices. The vial was then immersed for the required duration in a temperature-controlled oil bath pre-equilibrated to the required temperature: octadecene (200°C, 2h), octene (120°C, 24h), hexyne (70°C, 12h). After the reactions, samples were rigorously rinsed with gentle agitation in toluene (3x), chloroform (3x), and ultra-pure anhydrous ethanol (12x). Finally, samples were dried from ethanol using a dedicated (brand-new) critical point drier (Tousimis).

Gas-Phase Hydrosilylation of Alkene and Aldehyde The procedure was performed with the aid of a standard glass distillation head having 4 connection joints. The vacuum/inert gas inlet was connected to a turbo-molecular pump. The thermometer outlet was connected, via a valve, to an Ar line. A 20-ml pear-shaped flask containing 5 ml of octene and excess P_2O_5 (or octanal over excess 4 Å molecular sieves) was connected to the source joint. The distillate collection joint was temporarily closed with a small, 5-ml round-bottom flask. All joints were greased and gas-tight.

The alkene (aldehyde) was deoxygenated via 4 freeze-pump-thaw cycles under high vacuum and allowed to warm to room-temperature under Ar. Meanwhile, freshly H-terminated cantilever samples were quickly loaded into an aluminum foil-covered 10-ml pear-shaped flask (to minimize light-promoted re-oxidation during the $\approx$ 30 second air exposure during transfer). The sample flask was then attached to the distillate collection joint of the distillation head under moderate Ar flow. Ar flow was stopped and the system was immediately brought under high vacuum while the alkene source was simultaneously solidified in liquid nitrogen. After two additional rounds of freeze-pump-thaw cycles to remove dissolved Ar, the liquid was frozen and the system was brought under high vacuum one last time. Vacuum valve was closed, the alkene (aldehyde) was allowed to thaw and warm to room temperature, and the silicon sample flask was immersed into a 180°C oil bath for 6 hours. The alkene (aldehyde) source was maintained at room temperature throughout the process.

Reaction with propyne was performed inside a N_2 glovebox. Propyne from an as-purchased lecture bottle was used to fill a balloon. 10 ml pear-shaped flask was charged with about 0.5 g of anhydrous P_2O_5. The flask was closed by septum and gently flushed for 10 minutes with propyne gas from the balloon. During the flushing procedure, cantilever chips that had been mounted on a holder were H-terminated by the standard procedure and loaded into the glovebox with about 1 minute of air exposure during transport. The samples were inserted into the flask, which was quickly closed again. The cantilever holder piece ensured that the samples stayed well above the P_2O_5 powder by a couple of centimeters. Flushing was continued for 5 more minutes before removing the outlet needle. Flask was wrapped in aluminum foil and heated to 100°C overnight with the propyne balloon maintaining a slight positive pressure.

Two-step Alkylation and Amination Following H-termination, the samples were transferred to a nitrogen-flushed glove box maintained at 0.0% relative humidity. The samples were exposed to a vapor of dry (over excess P_2O_5) and deoxygenated Br_2 by creating a partial vacuum over the sample container before opening a valve to the Br_2 source. The brown Br_2 vapor was seen to immediately fill the sample container. The exposure lasted 30 minutes. Sample and the Grignard reagent solution (or dry, deoxygenated heptylamine) were added into 2-ml vials and sealed by clamped septum. The vials were heated to the required temperature and for the required duration: methyl magnesium bromide (3.2 M in 2-methyltetrahydrofuran, 90°C, 12h), 1-propenylmagnesium bromide (0.5 M in THF, 110°C, 24h), heptylamine (120°C, 12h). After the alkylation reactions, samples were rigorously rinsed with gentle agitation in THF (3x), methanol (3x), CH_2Cl_2 (3x), acetic

acid (3x), toluene (3x), chloroform (3x), and finally ultra-pure, anhydrous ethanol (12x) before drying from ethanol using a brand-new CPD. After the amination reaction, samples were rigorously rinsed with gentle agitation in CH_2Cl_2 (3x), toluene (3x), chloroform (3x), and finally ultra-pure, anhydrous ethanol (12x) before CPD drying from ethanol.

Thermal Nitridation using NH_3 was conducted using a commercial rapid thermal processing (RTP) system (Annealsys). The reactor chamber volume is roughly 2 liters. Sample is placed on a 4-inch silicon carrier wafer with 1 μm of thermal oxide. The temperature of the sample was assumed to be in equilibrium with that of the carrier wafer, which was monitored using a pyrometer. Within 30 seconds of the usual vapor HF treatment, cantilever and bulk-crystal samples were loaded, via brief air exposure, into the RTP chamber and immediately pumped down to a pressure below 10^{-5} mbar. The chamber was back-filled with Ar and evacuated again to below 10^{-5} mbar. Under vacuum, the sample was rapidly heated to 450°C at a constant 30% power over about 20 seconds. Temperature was allowed to stabilized to 450°C for 30 seconds under PID feedback. NH_3 was then introduced at a flow rate of 500 sccm for 30 seconds. Ammonia flow was decreased to 100 sccm and the chamber temperature was simultaneously ramped (>35°C/min) to the target temperature and held there for 60 seconds. Following the 60-second treatment, power supply to the heater was cut and the chamber temperature quickly fell to below 450°C. At this point, 100 sccm NH_3 flow was stopped and replaced with N_2 (purity 5.0) purge at 2000 sccm. The sample was allowed to cool to ambient temperature over several minutes under constant N_2 flow.

Thermal Nitridation using N_2 The same RTA and sample arrangement used for NH_3 nitridation were also used here. N_2 used in these experiments (except for the post-anneal cooling purge) was purchased at a purity of 6.0 and further purified at the point of use using an inline filter cartridge. Within 30 seconds of the usual vapor HF treatment, cantilever and bulk-crystal samples were loaded, via brief air exposure, into the RTP chamber and immediately pumped down to a pressure below 10^{-5} mbar. The chamber was back-filled with N_2 and evacuated again to below 10^{-5} mbar. N_2 was introduced at a flow rate of 1000 sccm for 60 seconds. N_2 flow was kept constant at 1000 sccm throughout the following steps. The sample was rapidly heated to 450°C at a constant 30% power over about 20 seconds and allowed to stabilized to 450°C for 5 seconds under PID feedback. The chamber temperature was ramped (>70°C/min) to the target temperature and held there for 60 seconds. Following the 60-second treatment, power supply to the heater was cut and the chamber temperature quickly fell to below 450°C. At this point 1000 sccm ultra-high purity N_2 flow was stopped and replaced with N2 (purity 5.0) purge at 2000 sccm. The sample was allowed to cool to ambient temperature over several minutes under a constant N_2 flow.

Cursory XPS examination showed substantial oxidation in addition to some nitrogen incorporation. Nitridation in N_2 is therefore a more finicky procedure than nitridation in NH_3. We have refrained from measurement the Q of N_2-nitrided samples in light of the XPS results.

Thermal Nitridation using N_2 and H_2 The treatment was conducted using a recipe similar to that for N_2 nitridation. The only difference is that 970 sccm N_2 and 30 sccm H_2 flows were used in place of the 1000 sccm N_2 flow.

Sample Characterization Mechanical properties of silicon nanoresonators were measured in a custom-built scanning force microscope originally designed for magnetic resonance force microscopy [36]. Cantilevers were prepared and mounted under ambient conditions and then mounted in a high-vacuum chamber ($< 10^{-6}$ mbar) at the bottom of a dilution refrigerator ($\sim 65\,\mathrm{mK} - 300\,\mathrm{K}$). Resonator frequency f_c and quality factor Q were measured using the ring-down method [3], and the spring constant k_c calibrated via a thermomechanical noise measurement at room temperature

[37]. As a consistency check f_c and k_c were independently calculated from the geometry using a finite element software (Comsol). Resonator motion was detected using a low-power fiber-optic interferometer [38] operating at a wavelength of 1550 nm and producing less than 10 nW of laser light incident at the cantilever. To exclude cavity effects, it was verified that the same Q factor was obtained whether the measurement was done on the positive or negative (red- or blue-shifted) side of the interferometer fringe. To measure temperature dependence of quality factors, temperature was measured the usual way by slowly ($\lesssim 0.2\,\mathrm{K/min}$) sweeping refrigerator temperature and assuming thermal equilibrium between resonator and bath.

4. Tabulation of Key Results

Some of the key results are given in Table 1.

Section	Material	Surface Treatment	$Q_{300K}(10^3)$ (σ)	$\frac{Q_{300K}}{Q_{300K\text{-}SiO_2}}$ (SE)[a]	$Q_{4K}(10^3)$ (σ)	$\frac{Q_{4K}}{Q_{4K\text{-}SiO_2}}$ (SE)	Air Stability Time Scale
0 Silicon and Oxides	Si wafer 1 + 2	None, Native Oxide	15.7 (5.7)	1	59 (26)	1	>months
	Si wafer 1 + 2	1000°C in Air, 20h	14.3 (4.0)	0.91 (0.42)	2.13 (0.25)	0.036(0.016)	>months
	Si wafer 1	UV-ozone/HF Vapor	115 (14)	7.3 (2.8)	343 (28)	5.8 (2.6)	<5 min
	Si wafer 2	UV-ozone/HF Vapor	32 (10)	2.0 (1.0)	317 (55)	5.4 (2.5)	<5 min
1 Thermal Nitridation	Si wafer 1	NH_3 600°C	24.5 (1.3)	**1.6 (0.6)**	108 (14)	**1.8 (0.8)**	days
	Si wafer 1	NH_3 700°C	25.8 (0.7)	**1.6 (0.6)**	114 (2)	**1.9 (0.9)**	days
	Si wafer 1	NH_3 800°C	23. (2)	**1.5 (0.5)**	121 (14)	**2.1 (0.9)**	days
	Si wafer 1	NH_3 1000°C	36.7 (0.4)	**2.3 (0.8)**	99 (3)	**1.7 (0.7)**	days
	LPCVD Si_3N_4	Commercial, As-Received	16.	N/A	38.	N/A	>months
2 Hydrosi-lylation	Si wafer 2	Liquid Octene on Si-H	24.5 (2.0)	**1.6 (0.6)**	188 (5)	**3.2 (1.4)**	≈ day
	Si wafer 2	Liquid Octadecene on Si-H	14.0 (1.9)	0.89 (0.35)	126 (7)	**2.1 (0.9)**	≈ day
	Si wafer 1 + 2	Liquid Hexyne on Si-H	10.7 (3.1)	0.68 (0.32)	125 (15)	**2.1 (1.0)**	≈ day
	Si wafer 1	Vapor Octanal on Si-H	41.6 (4.8)	**2.7 (1.0)**	186 (9)	**3.2 (1.4)**	≈ day
	Si wafer 1	Vapor Octene on Si-H	44.7 (7.6)	**2.8 (1.1)**	261 (22)	**4.4 (2.0)**	≈ day
	Si wafer 1	Vapor Propyne on Si-H	31.9(2.2)	**2.0 (.7)**	113 (6)	**1.9 (0.9)**	weeks
3 Traditional and Novel Silanization Protocols	Si wafer 1	$SiMe_2Cl_2$ on native oxide	18 (5)	1.1(0.5)	54 (6)	0.92 (0.42)	NA[b]
	Si wafer 1	$SiMe_2Cl_2$ on Si-H	39 (5)	**2.5 (1.0)**	57 (2)	1.0 (0.4)	>months
	Si wafer 1	$SiEt_2Cl_2$ on Si-H	32 (2)	**2.0 (0.8)**	ND[c]	NA	>months
	Si wafer 1	$SiMe_2HCl$ on Si-H	16.7 (2.0)[d]	1.1 (0.4)	ND	NA	NA
	Si wafer 1	TCTHPFOS[e] on Si-H	11.7 (0.5)	0.75 (0.27)	ND	NA	NA
	Si wafer 1	HMDS on Si-H	0.90 (0.09)	0.057 (0.022)	ND	NA	NA

Table 1: Quality factors of cantilevers follow various surface modifications All reported Q values are averages from between 5 to 46 measured cantilever devices. The corresponding standard deviations are in the parentheses. Significant improvements over native oxide-covered bench mark devices (Top entry) are marked in red and in bold. [a]: Standard errors in the Q ratios are dominated by the spread of Q values in the native-oxide covered devices, $Q_{\#K\text{-}SiO_2}$. [b]: Not Applicable, such as when Q values represent no improvement over native oxide baseline. [c]: Not Determined. [d]: Q decreased from 72 (28) to 16.7 (2.0) with 15 hours of air exposure. The kinetics of Q evolution suggest that no or little reaction had occurred with this mono-chloride. [e]: $Si(CH_2)_2(CF_2)_5CF_3Cl_3$;

5. Quality Factor vs Temperature for Some Important Samples

We have measured the temperature-dependences of Q of a commercial LPCVD Si_3N_4 cantilever and of a SiO_2 cantilever produced by thermal oxidation of a silicon device (Figure B). Given the additive nature of mechanical dissipation, this result suggests that replacing the native oxide by a nitride could improve the low-temperature Q of silicon cantilevers. This result is also the original motivation for investigating thermal nitridation methods.

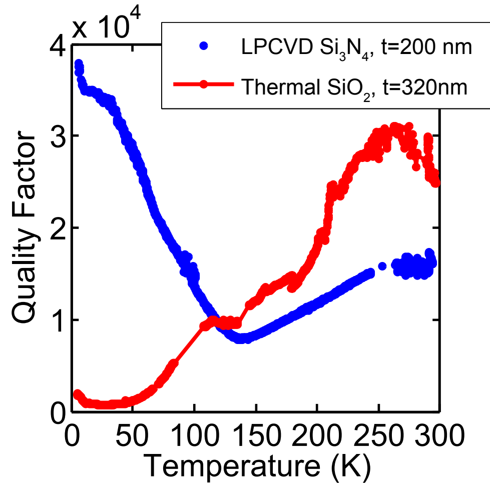

Figure B: Quality factors of a LPCVD Si_3N_4 cantilever and of a SiO_2 cantilever as a function of temperature.

Figure C plots the temperature dependance of mechanical quality factor for several important samples. The dip in Q between 10-20 K observed for the octene sample is most likely not related to the surface treatment, but is likely due to some defect in the bulk for that particular cantilever device. Similar dips has been observed in other samples on rare occasions.

In the main text, we attribute dissipation in the intermediate temperature range around 130K to carbonaceous adsorbates. We provide further evidence in Figure D that this might be the case. The plotted values are inverse quality factors, i.e., quantities proportional to mechanical dissipation. To compare the surface contributions, we have subtracted an upper-bound estimate of bulk dissipation represented by Q^{-1} of the Si-H device. The results show that the peak around 130K scales with the length of the carbon chain.

In Figure D, the two alkyl samples were prepared by liquid-phase methods, so may have higher non-specific surface contamination than the alkoxyl sample prepared in the gas-phase.

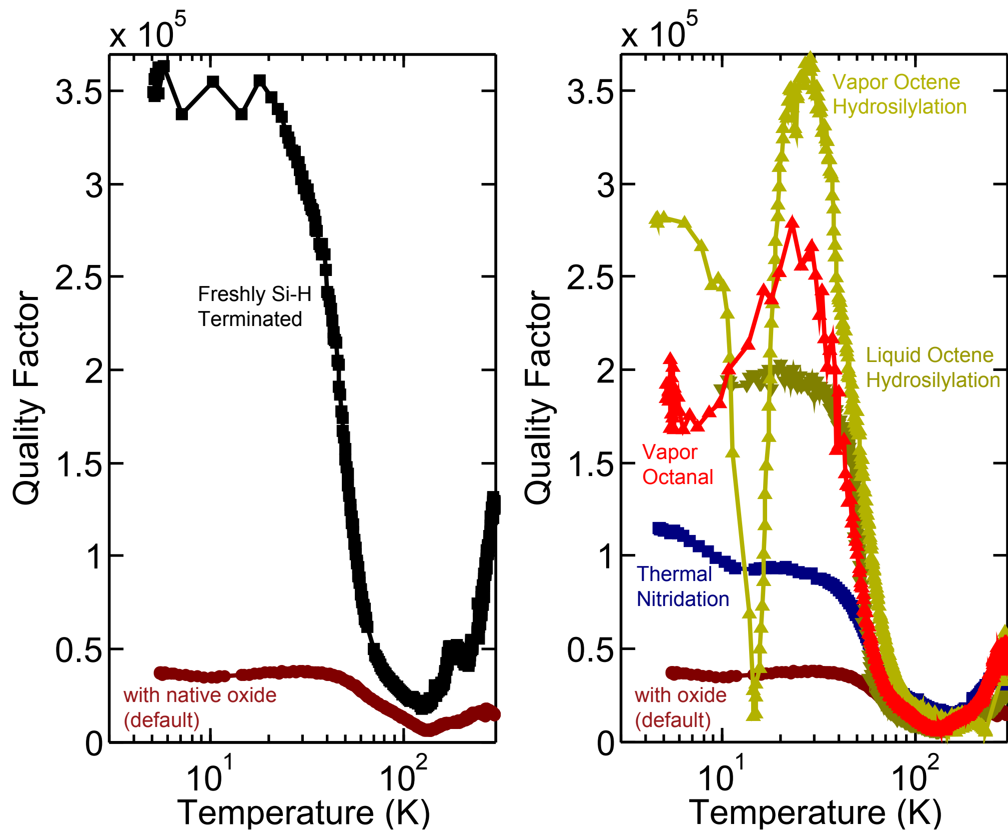

Figure C: The temperature-dependent quality factors of cantilevers with several key surface modifications.

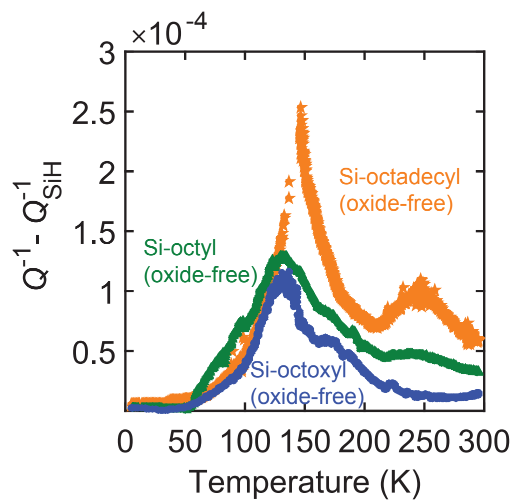

Figure D: Contributions of covalent carbonaceous monolayers and adventitious adsorbates to mechanical dissipation.

6. X-ray photoelectron spectroscopy (XPS) Analysis of Silicon Surfaces

Samples for XPS analysis were cut into 5mm x 5mm square chips from a bulk boron-doped Si⟨1,0,0⟩ wafer with resistivity between 1-10 Ohm cm. After dicing, the samples were cleaned by sonication in organic solvents, boiling in Piranha solution (10 minutes), extensive rinsing with deionized water, and blow-drying with nitrogen. They were then processed alongside silicon cantilever samples so that both the cantilever devices and the XPS monitor samples receive identical chemical modifications. Upon termination of chemical treatment, the samples were kept under high-purity (6.0) Ar gas for transportation to the XPS instrument (1-2 hours). They were finally analyzed following the indicated duration of air exposure (between opening of the Ar-filled container and start of pumpdown in the loadlock of the XPS instrument).

Detailed XPS studies were conducted for vapor HF-treated samples (Figure E, Table 2), hydrolilylated samples with octene (Figure F), thermal nitridation samples (Figure G, Table 3), SiH samples exposed to dichlorodimethylsilane vapor (Figure H, Tables 4 and 5), and SiH as well as native-oxide samples exposed to trichloro(1H,1H,2H,2H-tetrahydroperfluorooctyl) silane vapor (Figure I, Table 6). They are presented in this section. The determination of SiO_x thicknesses was based on methods described in reference [39].

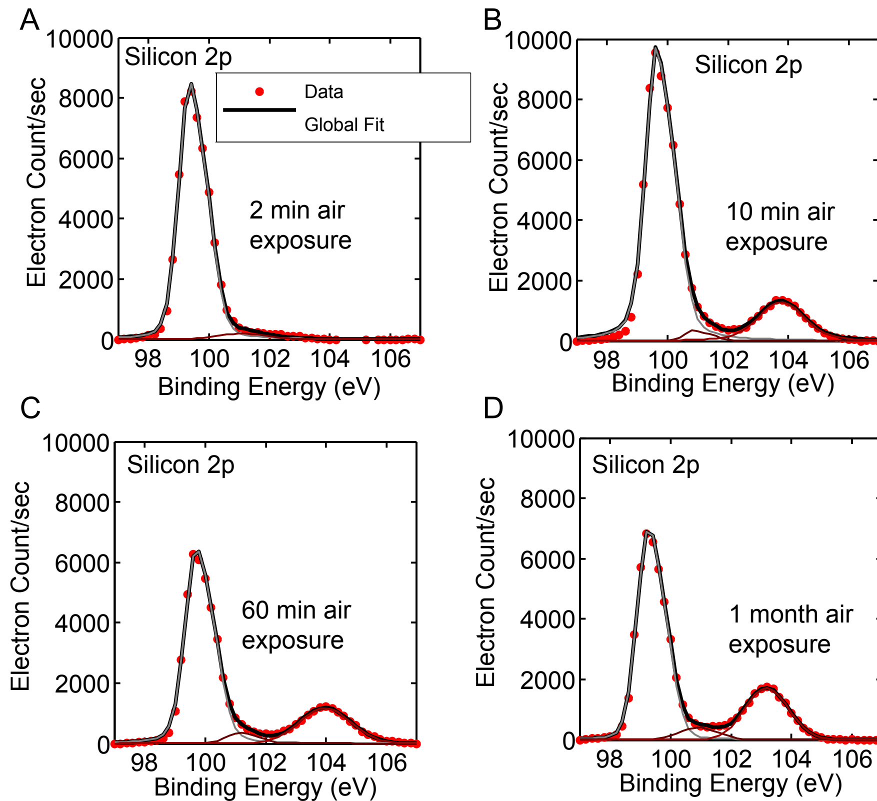

Figure E: XPS analysis of the ⟨1,0,0⟩ Si-H Surface prepared by vapor HF treatment as a function of ambient air exposure time. Data are for Si2p emission. **A**, 2 minutes of air exposure. **B**, 10 minutes of air exposure. **C**, 60 minutes of air exposure. **D**, 1 month of air exposure.

Air Exposure (Minutes)	SiO_x Total Area A.U.	Si Peak Area A.U.	SiO_x Thickness (nm)
2	48	1206	0.10
10	367	1458	0.58
60	342	943	0.80
48,000	428	979	0.94

Table 2: Summary of XPS analysis of the thicknesses of regrown native silicon oxides following vapor-phase H-termination and air exposure; Raw data and fits are presented in Figure E.

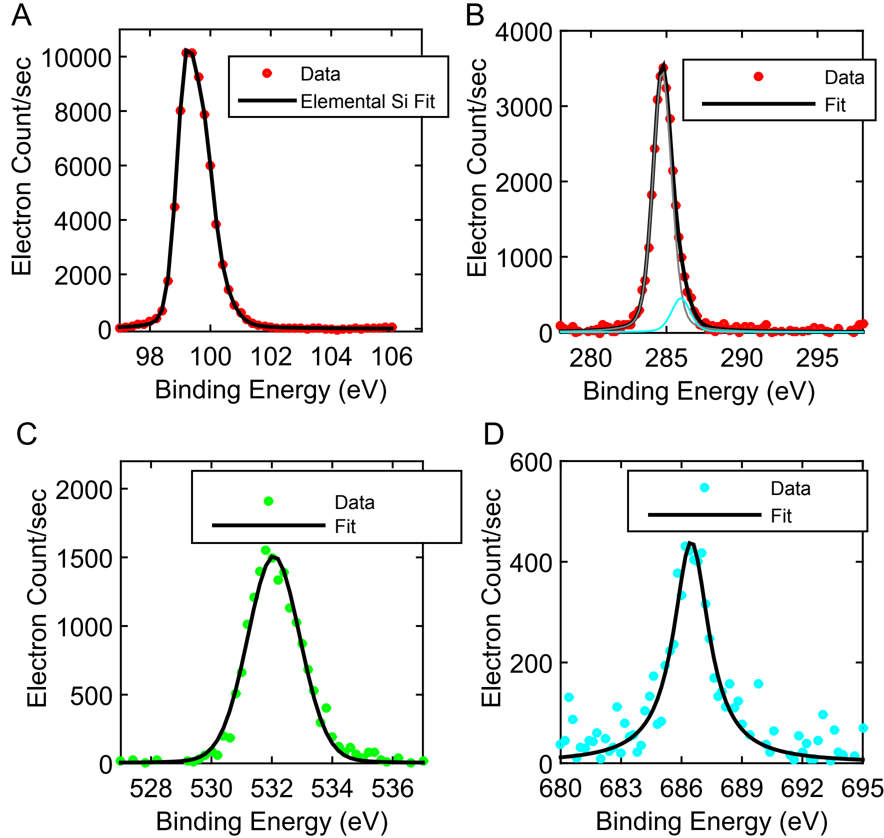

Figure F: XPS analysis of the ⟨1,0,0⟩ Si-Octyl Surface prepared by vapor octene exposure of Si-H surface. Sample was analyzed with less than 2 hours of air exposure post-preparation . **A**, Silicon 2p peak showing absolutely no oxide contribution. **B**, Carbon 1s peak and fit. Carbon signal is from both covalently attached and physisorbed species. **C**, Oxygen 1s peak and fit. Oxygen contribution is entirely from adsorbates. **D**, Fluorine 1s peak and fit. The fluorine is likely a residue from the HF treatment.

Process Temperature (°C)	SiO_x Total Area A.U.	Si Peak Area A.U.	SiO_xN_y Thickness (nm)	N1s Area A.U.	O1s Area A.U.	% Nitrogen (min Estimate)
600	569	1698	0.75	307	1329	25
700	607	1131	1.11	579	988	46
800	716	985	1.40	940	979	59
1000	1089	651	2.51	1753	1032	71

Table 3: Summary of XPS analysis of the thicknesses and compositions of oxynitrides formed on Si-H surface during thermal nitridation in NH_3. For nitrogen content as a percentage of total nitrogen and oxygen content, we have divided the raw measured peak areas by the relative sensitivity factors (RSF) of the emitting orbitals: 0.499 for N1s and 0.733 for O1s. Raw data and fits are presented in Figure G.

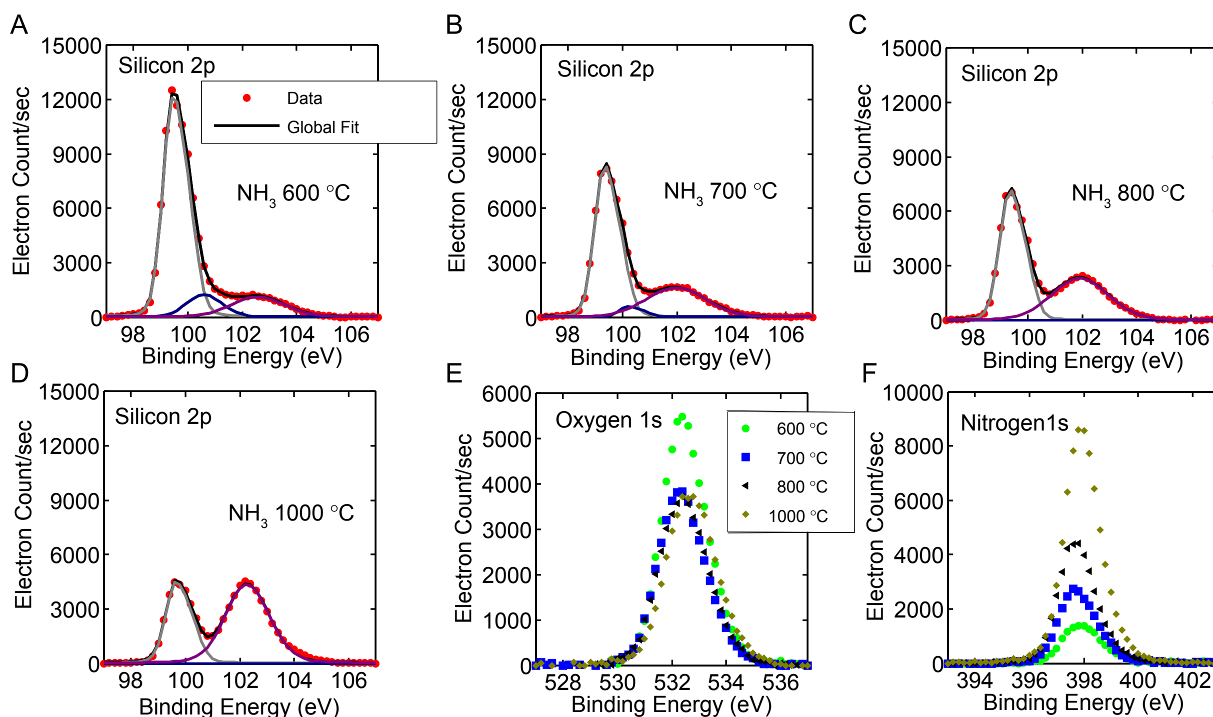

Figure G: XPS analysis of Si ⟨1,0,0⟩ following thermal nitridation of Si-H surfaces in NH_3. **A-D**, Si2p peaks for nitridation at 600°C, 700°C, 800°C, and 1000°C. **E**, O1s peaks for the same samples. **F**, N1s peaks for the same samples. The spectra are taken after 3 hours of air exposure after the nitridation procedure.

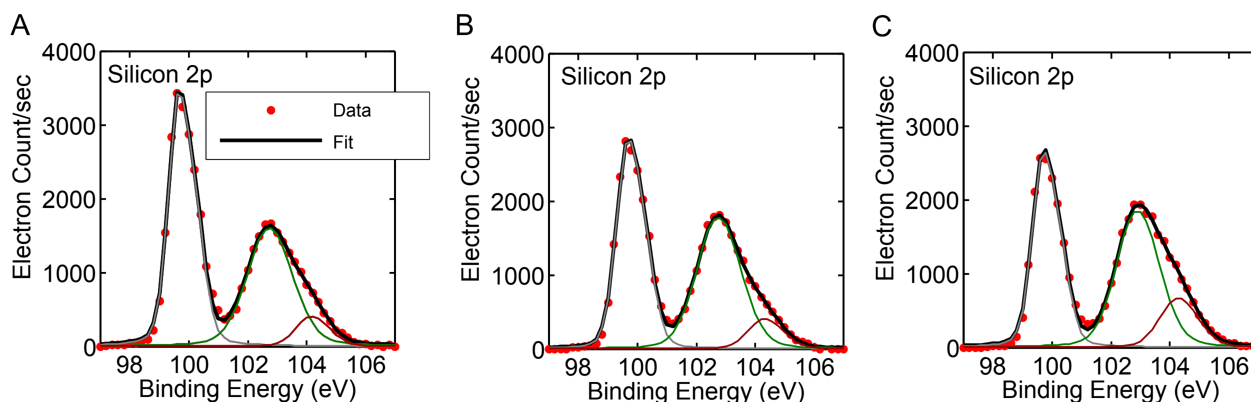

Figure H: XPS analysis of the ⟨1,0,0⟩ Si-H surface after treatment by vapor-phase dichlorodimethylsilane as a function of ambient air exposure time. Data are for Si2p emission. **A**, 10 minutes of air exposure. **B**, 60 minutes of air exposure. **C**, 900 minutes of air exposure.

For dichlorodimethylsilane-treated samples, we also performed an analysis of the relative atomic concentrations of carbon (C1s), oxygen (O1s), and silicon (Si2p) to confirm that the none-SiO_x component is consistent with a species with empirical formula $(SiMe_2O)_n$.

Air Exposure (Minutes)	SiO_2 Peak Area A.U.	-O-$SiMe_2$-O- Peak Area A.U.	Si Peak Area A.U.	Polydimethylsiloxane (nm)	SiO_2 Thickness (nm)
10	1171	2515	4351	0.96	0.62
60	1257	2671	3734	1.09	0.75
900	1388	2720	3756	1.08	0.81

Table 4: Summary of XPS analysis of the thicknesses and compositions of polydimethylsiloxane thin film formed on Si-H surface by vapor phase exposure to dichlorodimethylsilane, as a function of air exposure time. Raw data and fits are presented in Figure H.

Air Exposure (Minutes)	Total C Atomic %	Total O Atomic %	Total Si Atomic %	Si: SiO_2 Atomic %	**Si: $SiMe_2O$** Atomic %	**C: $SiMe_2O$** Atomic %	C: Adsorbates Atomic %	**O: $SiMe_2O$**[1] Atomic %
10	29.1	34.4	36.5	5.9	12.7	25.5	2.8	15.8
60	31.6	30.6	36.8	6.0	12.8	25.7	6.0	12.6
900	28.3	30.5	40.7	6.4	12.6	25.3	3.8	17.7

Table 5: Summary of surface atomic concentration analysis, confirming the empirical formula of the thin film obtained by treating Si-H with dichlorodimethylsilane vapor to be that of polydimethylsiloxane: $(SiMe_2O)_n$. [1] These values are calculated assuming oxygen has the same level of contamination as carbon. Therefore, the values are the maximum amount of oxygen that could be found in the polymer film.

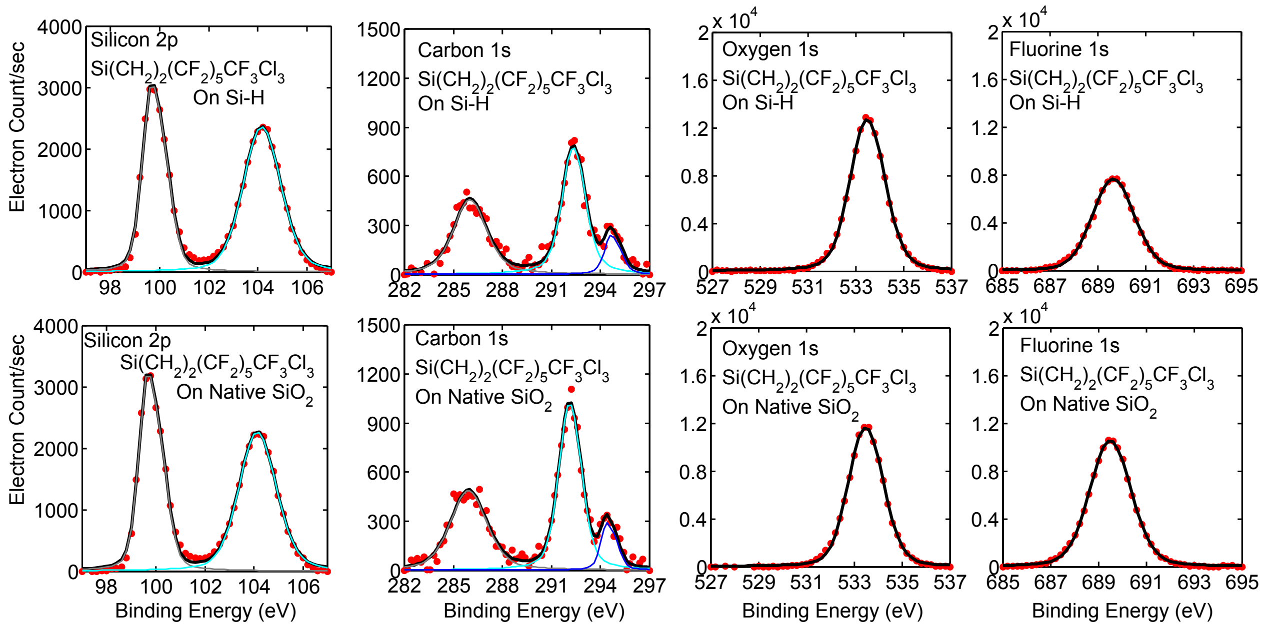

Figure I: XPS analysis of ⟨1,0,0⟩ Si-H surface (Top Row) and ⟨1,0,0⟩ Si surface with normal native oxide (Bottom Row) after treatment by vapor-phase trichloro(1H,1H,2H,2H-tetrahydroperfluorooctyl) silane. The silicon signals are satisfactorily fitted to 2 components. The carbon signal was fitted to 3 components, as expected. The oxygen and fluorine signals are well-modeled by single peaks.

Sample		Total C	Total F	Total O	Si: Crystal	Si: SiO_x	SiO_x (nm)	SiO_2 (nm)	O_3Si-R SiO_2-equi. (nm)
Vapor On	Atomic Percent	11.5	19.3	37.3	11.7	14.6			
Si-H	Normalized to F	8.9	15	29.	9.1	11.4	2.07	1.94	0.13
Vapor On	Atomic Percent	13.5	26.5	33.7	12.2	14.1			
Native Oxide	Normalized to F	7.6	15	19.	6.9	7.9	1.96	1.79	0.17

Table 6: Summary of surface atomic concentration analysis of trichloro(1H,1H,2H,2H-tetrahydroperfluorooctyl) silane vapor-treated samples. Results confirm the formation of a fluoroalkyl monolayer on both types of starting surfaces. Compared to the structure formed on already-formed native oxide surface, the oxide grown from a Si-H surface appears slightly thicker and its surface fluoroalkyl monolayer, slightly less densely-packed.

7. Frequency and Quality Factor Data from Cyclic Oxide Removal-Native Oxidation Experiments

The devices used in this experiment come from Wafer 2 (see Table 1), which displayed lower Q at room temperature in the Si-H state.

Device	1 f (Hz)	1 Q	2 f (Hz)	2 Q	3 f (Hz)	3 Q	4 f (Hz)	4 Q	5 f (Hz)	5 Q
DF 1	8442.8	36692	7027.8	37564	5845.2	37224	5682.0	34703	6850.0	31214
Air 1	8435.6	26735	7022.5	28214	5840.9	27923	5677.5	26064	6844.9	24499
DF 2	8420.5	36715	7010.6	35761	5831.8	34986	5665.8	34150	6823.4	33093
Air 2	8413.6	27268	7005.3	28215	5827.5	27816	5661.4	26370	6818.3	25924
DF 3	8405.1	35464	6999.2	36245	5822.5	34711	5656.2	34082	6819.4	32280
Air 3	8399.3	27075	6994.6	27925	5818.7	27294	5652.5	26438	6815.0	25262
DF 4	8322.3	34496	6964.3	35100	5786.4	34673	5632.4	33632	6792.4	31233
Air/Dark	8320.6	30056	6962.8	31058	5785.2	30860	5631.2	30017	6791.0	28475
HF 1	8315.6	30936	6950.4	31552	5777.4	33290	5626.5	34372	6799.3	28629
Air 5	8307.5	25214	6945.8	27258	5773.8	26747	5623.0	28899	6796.6	23554
HF 2	8265.6	27108	6919.8	27073	5752.3	31873	5603.7	32623	6769.4	24605

Table 7: Frequency and room-temperature quality factor evolution during cyclic DF/HF exposure and 1h air oxidation experiments.

In the present study, XPS measurements show negligible amount of silicon oxides remaining on the surface right after each hydrofluoric acid vapor step. In this oxide-free state, the mechanical frequency of the cantilever is directly proportional to the silicon crystal thickness. The ratio of frequencies between two successive DF treatment steps thus reflect the ratio of bare silicon thicknesses between those steps. The initial cantilever thicknesses are precisely known from fabrication, SEM characterization, and Comsol simulation. Without distinguishing the suboxides (maximum 0.12 nm per cantilever side [39]) from the dioxide, one can thus obtain the thickness of silicon lost as silicon oxides after each air-oxidation/DF cycle. This value in turn gives the thickness of corresponding native oxide film that had been present on the surface before vapor-phase removal. As a result, all quantities in Equation (1) of main text, with the exception of E_{SiO_2}, can be directly obtained from the data or literature. As shown in the main text, the data is consistent with theoretical predictions of a Si/SiO$_x$ bimorph cantilever, with a native oxide film having a thickness-independent, in-plane Young's modulus of 97.1±1.7 GPa (assuming density is the same as for bulk fused quartz).

We note the presence of randomness in the thickness of oxide regrowth over different 1-h periods and among different devices on the same sample chip. Due to the marked dependence of native oxidation rate on various environmental factors like relative humidity, lighting, and temperature, this level of spread is to be expected for an experiment conducted over several days in our laboratory without temperature or humidity control. To our knowledge, this study is the first direct experimental determination of the Young's modulus of sub-nm-thin native SiO_2 films.

8. Si and SiO_2 Material Properties Used in Data Analysis

In order to derive the Youngs' modulus of native oxide films from measured cantilever frequency data, we used the following material constants: $E_{\mathrm{Si}} = 171$ GPa, $\rho_{\mathrm{SiO_2}} = 2.203$ g/cm^3, and $\rho_{\mathrm{Si}} = 2.329$ g/cm^3. In the calculation, we assume that the density of the native oxide is the same as that of fused quartz. This assumption is equivalent to neglecting the presence of suboxides, which are expected to have densities between those of silicon and fused quartz, thus higher than the value for fused quartz. We also assume that the thickness of grown oxide to be directly proportional to the thickness of lost silicon crystal, via a proportionality constant of 2.27 based on the volume expansion in the reaction from Si to SiO_2.

9. Oxide Growth Underneath Polydimethylsiloxane Thin Film

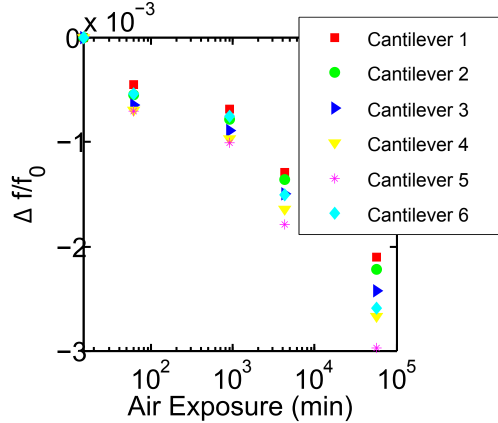

Figure J: Fractional frequency change of cantilevers that had been exposed to dichlorodimethylsilane (DCDMS) vapor as a function of post-treatment air exposure.

XPS measurements show that surface oxide formation in the presence of DCDMS vapor lead to a 1 nm polydimethylsiloxane film covering a native oxide on top of crystalline silicon. XPS also shows that when exposed to air, the oxide layer underneath this thin polymer film continues to grow. When DCDMS-treated cantilevers were monitored over a 40-day air exposure period, monotonic decrease in resonance frequencies was observed, suggesting continued thickening of the oxide layer (Figure J, Table 8). Here, we analyze the cantilever frequency data to extract the temporal evolution of SiO_2 thickness and the Young's modulus of the underlying oxide film formed in such a 'template-directed' native oxidation process.

We can neglect the 1 nm polydimethylsiloxane in the following analysis. We are justified to do so as long as its structure does not significantly change over time, so that its presence merely adds a small (relative to the resonance frequency) constant value to all measured frequencies. XPS measurements have confirmed that the thickness of this polymer film is constant in time.

We consider the sample upon the first frequency measurement as the reference and calculate additional SiO_2 growth compared to this initial measurement. Let the thickness of the silicon core and the measured frequency at the first measurement be t_0 and f_{0m}, respectively. We call f_0 the frequency that one would measure had it been possible to selectively remove the polydimethylsiloxane film and the initially-formed underlying oxide of thickness $t_{\mathrm{SiO_2}0}$, leaving only the silicon core of thickness t_0. Such a procedure is obviously not yet possible to achieve experimentally. To proceed further, we therefore need to express f_0 as a function of measured values f_{0m} and $t_{\mathrm{SiO_2}0}$, the oxide thickness upon first measurement.

The measured initial frequency, f_{0m}, is related to f_0 via $f_{0m} = f_0 + \Delta f_0$, where

$$\Delta f_0 = \left(\frac{3E_{\mathrm{SiO_2}}}{2E_{\mathrm{Si}}} - \frac{\rho_{\mathrm{SiO_2}}}{2\rho_{\mathrm{Si}}}\right)\frac{t_{\mathrm{SiO_2}0}}{t_0} f_0 \equiv \alpha \frac{t_{\mathrm{SiO_2}0}}{t_0} f_0 \tag{1}$$

Here, E and ρ are the Young's moduli and material densities. Therefore,

$$f_0 = \left(1 + \alpha \frac{t_{\mathrm{SiO_2}0}}{t_0}\right)^{-1} f_{0m} \tag{2}$$

When an additional oxide thickness, $\Delta t_{\mathrm{SiO_2}}$, grows on the cantilever, the silicon core reduces in

thickness to a value

$$t = t_0 - \frac{\Delta t_{SiO_2}}{\beta} \quad (3)$$

where $\beta = 2.27$ is the volume expansion factor when silicon oxidizes to fused quartz. Due to the constrained geometry in a surface thin film, this volume expansion is confined to the thickness dimension perpendicular to the film surface.

At later measurements, we measure a frequency $f_m = f + \Delta f$, where f, analogous to f_0, would be the frequency of a cantilever had we been able to selectively remove the oxide, and Δf is the contribution of the oxide layer to the experimentally accessible f_m. Similar to f_0, f is beyond experimental reach, but can be expressed as $f = \frac{t}{t_0} f_0$ based on the scaling of frequency with cantilever thickness. Eliminating f from the expression for f_m, we have

$$f_m = \frac{t}{t_0} f_0 + \Delta f \quad (4)$$

Δf is found similarly to Δf_0:

$$\Delta f = (\frac{3E_{SiO_2}}{2E_{Si}} - \frac{\rho_{SiO_2}}{2\rho_{Si}})\frac{t_{SiO_2}}{t} f \equiv \alpha \frac{t_{SiO_2}}{t} f = \alpha \frac{t_{SiO_2}}{t_0} f_0 \quad (5)$$

Combining Equations (2) to (5) and solving for Δt_{SiO_2} we have,

$$\Delta t_{SiO_2} = \frac{[\frac{f_m}{f_{m0}}(1 + \alpha \frac{t_{SiO_20}}{t_0}) - 1]t_0 - \alpha t_{SiO_20}}{\alpha - \frac{1}{\beta}}. \quad (6)$$

It is clear that because t_{SiO_20} is vanishingly small compared to t_0, the value of Δt_{SiO_2} is practically independent of the value of t_{SiO_20} one enters into the equation. For consistency, we use the value of 0.62 nm as determined by XPS in Table 4. $t_0 = 115$ nm is known from fabrication and confirmed by SEM inspection as well as Comsol simulations. Therefore, Δt_{SiO_2} only depends on α, a parameter that summarizes the material properties. We had previously determined the Young's modulus of natural native oxide to be 97.1(1.7) GPa, corresponding to $\alpha = 0.379$. However, it is not valid to assume that an oxide formed under a 1-nm polydimethylsiloxane should have the same materials properties as the natural native oxide. Therefore, we used the XPS data presented in Table 4 to calibrate the frequency change data. The calibration gives $E_{SiO_2} = 74.7$ GPa, corresponding to $\alpha = 0.181$. This value for the Young's modulus is very close to commonly reported values of amorphous quartz. The differences in the Young's moduli and dissipation of surface oxides formed under difference conditions may suggest differences in their atomic structures.

Device	f (Hz) 10 min Air	Q 10 min Air	f (Hz) 1 h Air	Q 1 h Air	f (Hz) 15 h Air	Q 15 h Air	f (Hz) 3 days Air	Q 3 days Air	f (Hz) 40 days Air	Q 40 days Air
1	7374.5	38580	7371.2	36061	7369.5	37778	7365.0	37077	7359.0	36301
2	6023.0	35966	6019.7	32127	6018.3	35186	6014.8	33102	6009.6	33255
3	4974.3	37441	4971.1	33807	4969.9	36259	4966.9	34649	4962.2	34307
4	4969.4	40040	4966.0	37778	4964.6	40815	4961.2	38297	4956.1	38174
5	5999.1	44181	5994.9	38407	5993.1	42545	5988.3	39002	5981.3	39715
6	7443.2	44429	7439.2	38543	7437.6	43156	7432.0	38101	7423.9	38059

Table 8: Frequency and room-temperature quality factor evolution of DCDMS vapor-treated cantilevers Devices 1 and 6, 2 and 5, 3 and 4 are 90, 105, and 120 μm long, respectively.

10. Other Tested Silicon Surface Modification Strategies With Results That May be Optimized

10.1. Two-Step Alkylation and Amination Reactions (IIa)

These experiments are based on the now-standard halogenation/alkylation sequence first reported by Bansel et. al. [23]. These two-step procedures did not lead to improvement in Q. In the alkylation case, we attribute the result to visible reaction residues on the silicon surface due to inability to apply ultrasonic assistance during post-reaction solvent rinsing and cleaning (fragile cantilevers break instantaneously even with weak sonicator power).

Device From	Surface Treatment	$Q_{300K}(10^3)$ (σ)	$\frac{Q_{300K}}{Q_{300K\text{-}SiO_2}}$ (SE)^a	$Q_{4K}(10^3)$ (σ)	$\frac{Q_{4K}}{Q_{4K\text{-}SiO_2}}$ (SE)	Air Stability Time Scale
Si wafer 2	Heptylamine on Si-Br	12.2 (1.6)	0.78 (0.30)	55 (17)	0.93 (0.50)	NA
Si wafer 2	MeMgBr on Si-Br	6.3 (1.0)	0.40 (0.16)	52 (12)	0.88 (0.44)	NA
Si wafer 1	Allyl MgBr on Si-Br	9.3 (0.9)	0.59 (0.22)	46 (4)	0.78 (0.35)	NA

Table 9: Quality factors of cantilevers following 2-step alkylation/amination procedures

10.2. Spontaneous Diazonium Salt Grafting (IIa)

This experiment was based on results in [40], where immersion of silicon <1,0,0> wafers into a solution of diazonium salt and HF (2%) in CH_3CN/H_2O (1:1) led to native oxide removal and the deposition of an organic thin film of controllable thickness (by adjusting reaction time). Based on Table 1 in [40], we chose to use an Ar-sparged 4-bromobenzenediazonium tetrafluoroborate (0.20 mM) solution in 2% HF in CH_3CN/H_2O (1:1) and a reaction time of 10 minutes.

We first established a method for reversibly dipping the cantilevers into a liquid and retracting them back into the air. The cantilever chip was mounted, tip pointing down, on a micromanipulator. The vertical movement of the sample could be controlled with about 5 μm accuracy by constantly monitoring the sample through a microscope. The sample was positioned over a small Teflon beaker of Ar-sparged 2% HF in 50% CH_3CN. The cantilevers shafts were lowered into the liquid (until 10 μm from the base) for 5 seconds and quickly retracted up, out of the liquid. It is essential to preventing the liquid from getting into contact with the base of the cantilevers, i.e. the silicon chip. Because otherwise, surface tension would cause the liquid to climb up and completely cover the small sample chip. If this wetting happens, tedious critical-point drying becomes necessary.

The frequencies and Qs measured following 5-min air exposure confirmed successful SiO_2 removal. The sample was then mounted back onto the micromanipulator and immersed into the 0.20 mM 4-bromobenzenediazonium tetrafluoroborate solution for 10 minutes. The sample was remeasured after the grafting reaction. Results in Table 10 suggest formation of a rather thick coating on the cantilevers. The color of the cantilevers in areas that had been exposed to the liquid vs areas that had stayed dry were markedly different, confirming the formation of a thick film.

Due to difficulties associated with precise control of coating thickness, this methods has not been pursued further. Future studies should consider a dedicated setup inside a glovebox to eliminate potential complications such as O_2-promoted polymerization and oxidation.

10.3. Atomic Layer Deposition (ALD) of Al_2O_3 (IIc)

Samples were H-terminated as usual and loaded into a commercial ALD system with <1 min air exposure during transfer. Al_2O_3 coating (10 cycles) was performed with 0.1 second reagent pulses and 4 sec pumping steps at a temperature of 110 °C. Measurements at room temperature were performed following 20 minutes and 2 hours of air exposure. The significant decrease in both frequency and quality factor points to the inefficiency of the treatment at preventing oxidation. Future efforts along

Device	f (Hz) 2% HF Dip w/o Diazonium	Q (300 K) 2% HF Dip w/o Diazonium	f (Hz) Immersion w/ Diazonium	Q (300 K) Immersion w/ Diazonium
1	7,593	61,331	6,281	3,513
2	6,124	61,138	4,873	2,544
3	5,048	49,723	3,870	2,544
4	5,340	53,018	4,217	2,239
5	7,478	53,398	6,180	3,219

Table 10: Results for spontaneous diazonium alkylation;

this direction should consider thicker ALD films and alternative materials.

Device	f (Hz) 20 min Air	Q (300 K) 20 min Air	f 2 h Air	Q 2 h Air
1	4313.97	20,591	4301.21	16,657
2	5091.05	22,282	5078.02	17,391
3	6342.76	17,428	6328.70	14,496
4	7305.94	22,791	7289.43	17,356

Table 11: Results for ALD Al_2O_3 coating;

10.4. Electron Beam Evaporation of Al_2O_3 (IIc)

Samples were H-terminated as usual and loaded into the evaporator loadlock with <2 min air exposure during transfer. 2.0 nm of Al_2O_3 were evaporated onto each side of the cantilevers at a rate of 0.10 nm/sec. Measurements were performed following 20 minutes air exposure. The results show significant dissipation from the thin Al_2O_3 film at room temperature. The cantilever also appeared to have slight curvature, indicating residual, unbalanced stress from the coatings. Variable-temperature measurement was not undertaken.

Material	Sample Size	$Q(10^3)$ (300 K) (Standard Deviation)
Si Wafer 1	6	10.0(0.4)
Si Wafer 2	6	12.7 (0.3)

Table 12: Results for ebeam evaporated Al_2O_3 thin coating;

10.5. Simultaneous Exposure to HF Vapor and Alkene Vapor

We have subjected UV/Ozone-cleaned cantilever devices and silicon wafer dies to a gas mixture of wet HF vapor and alkene vapor (pentene, hexene, or heptene). The motivation of the experiment was to test whether the constant presence of HF vapor could maintain the silicon surface in an oxide-free state for the alkene to react with until saturation coverage was reached. The resulting surfaces were highly hydrophobic, suggesting the formation of a hydrocarbon top layer. XPS analysis showed the presence of substantial SiO_2 (1-2 nm) underneath a carbon-rich thin layer (data not presented here). The quality factors of the cantilevers were similar to those of the default, native oxide-covered devices. The results may suggest that the alkene can react with SiO_2 in the presence of HF and H_2O, perhaps via acid-catalyzed electrophilic addition to form Si-O-R. The surface alkyl layer may then protect the underlying oxide from attack by HF vapor.

References

[1] Deal, B. E. and Grove, A. S. *J. Appl. Phys.* **36**, 3770–3778 (1965).
[2] Henry, J. A., Wang, Y., and Hines, M. A. *Applied Physics Letters* **84**, 1765–1767 (2004).
[3] Yasumura, K. Y., Stowe, T. D., Chow, E. M., Pfafman, T., Kenny, T. W., Stipe, B. C., and Rugar, D. *J. Microelectromech. Sys.* **9**, 117–125 (2000).
[4] Webb, L. J. and Lewis, N. S. *J. Phys. Chem. B* **107**, 5404–5412 (2003).
[5] Popoff, R. T. W., Asanuma, H., and Yu, H.-Z. *J. Phys. Chem. C* **114**, 10866ï£¡–10872 (2010).
[6] McKee, R. A., Walker, F. J., and Chisholm, M. F. *Phys. Rev. Lett.* **81**, 3014ï£¡–3017 (1998).
[7] Kingon, A. I., Maria, J.-P., and Streiffer, S. K. *Nature* **406**, 1032–1038 (2000).
[8] Evans, J. W. and Chatterji, S. K. *J. Phys. Chem.* **62**, 1064–1067 (1958).
[9] Hayafuji, Y. and Kajiwara, K. *J. Electrochem. Soc.* **129**, 2102–2108 (1982).
[10] Green, M. L., Sorsch, T., Feldman, L. C., Lennard, W. N., Gusev, E. P., Garfunkel, E., Lu, H. C., and Gustafsson, T. *Appl. Phys. Lett.* **71**, 2978–2980 (1997).
[11] Morita, Y., Ishida, T., and Tokumoto, H. *Jpn. J. Appl. Phys.* **41**, 2459ï£¡–2462 (2002).
[12] Linford, M. R. and Chidsey, C. E. D. *J. Am. Chem. Soc.* **115**, 12631–12632 (1993).
[13] Cicero, R. L., Linford, M. R., and Chidsey, C. E. D. *Langmuir* **16**, 5688–5695 (2000).
[14] Cicero, R. L. and Chidsey, C. E. D. *Langmuir* **18**, 305–307 (2002).
[15] Sun, Q.-Y., de Smet, L. C. P. M., van Lagen, B., Wright, A., Zuilhof, H., and Sudhölter, E. J. R. *Angew. Chem. Int. Ed.* **43**, 1352–1355 (2004).
[16] Liu, Y., Yamazaki, S., Yamabe, S., and Nakato, Y. *J. Mat. Chem.* **15**, 4906ï£¡–4913 (2005).
[17] Scheres, L., Arafat, A., and Zuilhof, H. *Langmuir* **23**, 8343–8346 (2007).
[18] Ng, A., Ciampi, S., James, M., Harper, J. B., and Gooding, J. J. *Langmuir* **25**, 13934–13941 (2009).
[19] Scheres, L., Giesbers, M., and Zuilhof, H. *Langmuir* **26**, 4790–4795 (2010).
[20] Zhong, Y. L. and Bernasek, S. L. *J. Am. Chem. Soc.* **133**, 8118ï£¡–8121 (2011).
[21] Cicero, R. L. and Chidsey, C. E. D. *Langmuir* **28**, 6577–6588 (2012).
[22] Eves, B. and Lopinski, G. *Surface Science* **579**, L89ï£¡–L96 (2005).
[23] Bansal, A., Li, X., Lauermann, I., Lewis, N. S., Yi, S. I., and Weinberg, W. H. *J. Am. Chem. Soc.* **118**, 7225–7226 (1996).
[24] Wong, K. T. and Bent, S. F. *Oxford Handbook of Innovation*, chapter Pericyclic Reactions of Organic Molecules at Semiconductor Surfaces. John-Wiley & Sons, Inc., Hoboken, New Jersey (2012).
[25] de Villeneuve, C. H., Pinson, J., Bernard, M. C., and Allongue, P. *J. Phys. Chem. B* **101**, 2415–2420 (1997).
[26] Gurtner, C., Wun, A. W., and Sailor, M. J. *Angew. Chem. Int. Ed.* **101**, 1966–1968 (1999).
[27] Robins, E. G., Stewart, M. P., and Buriak, J. M. *Chem. Commun.* , 2479ï£¡–2480 (1999).
[28] Stewart, M. P., Maya, F., Kosynkin, D. V., Dirk, S. M., Stapleton, J. J., McGuiness, C. L., Allara, D. L., and Tour, J. M. *J. Am. Chem. Soc.* **126**, 370–378 (2004).
[29] Effenberger, F., Götz, G., Bidlingmaier, B., and Wezstein, M. *Angew. Chem. Int. Ed.* **37**, 2462–2464 (1998).
[30] Boukherroub, R., Morin, S., Sharpe, P., Wayner, D. D. M., and Allongue, P. *Langmuir* **16**, 7429–7434 (2000).
[31] *Atomic-Scale Mechanistic Study of Iodine/Alcohol Passivated Si(100)*, October (1999).
[32] Bergerson, W. F., Mulder, J. A., Hsung, R. P., and Zhu, X.-Y. *J. Am. Chem. Soc.* **121**, 454–455 (1999).
[33] Tian, F., Taber, D. F., and Teplyakov, A. V. *J. Am. Chem. Soc.* **133**, 20769ï£¡–20777 (2011).
[34] Leftwich, T. R., Madachik, M. R., and Teplyakov, A. V. *J. Am. Chem. Soc.* **130**, 16216ï£¡–16223

(2008).
[35] Chui, B. W., Hishinuma, Y., Budakian, R., Mamin, H. J., Kenny, T. W., and Rugar, D. *The 12th International Conference on Solid Stale Sensors, Actuators and Microsystems* **2**, 1120–1123 (2003).
[36] Rugar, D., Budakian, R., Mamin, H. J., and Chui, B. W. *Nature* **430**, 329 (2004).
[37] Stowe, T. D., Yasumura, K., Kenny, T. W., Botkin, D., Wago, K., and Rugar, D. *Appl. Phys. Lett.* **71**, 288–290 (1997).
[38] Rugar, D., Mamin, H. J., and Guethner, P. *Appl. Phys. Lett.* **55**, 2588–2590 (1989).
[39] Seah, M. P., Spencer, S. J., Bensebaa, F., Vickridge, I., Danzebrink, H., Krumrey, M., Gross, T., Oesterle, W., Wendler, E., Rheinlander, B., Azuma, Y., Kojima, I., Suzuki, N., Suzuki, M., Tanuma, S., Moon, D. W., Lee, H. J., Cho, H. M., Chen, H. Y., Wee, A. T. S., Osipowicz, T., Pan, J. S., Jordaan, W. A., Hauert, R., Klotz, U., van der Marel, C., Verheijen, M., Tamminga, Y., Jeynes, C., Bailey, P., Biswas, S., Falke, U., Nguyen, N. V., Chandler-Horowitz, D., Ehrstein, J. R., Muller, D., and Dura, J. A. *Surface and Interface Analysis* **36**, 1269–1303 (2004).
[40] Chen, B., Flatt, A. K., Jian, H., Hudson, J. L., and Tour, J. M. *Chem. Mater.* **17**, 4832–4836 (2005).